Assessment of ride safety based on the wind-traffic-pavement-bridge coupled vibration

Yin Xinfeng[1a], Liu Yang[*1] and Chen S.R.[1,2b]

[1]*School of Civil Engineering and Architecture, Changsha University of Science & Technology, Changsha 410004, Hunan, China*
[2]*Department of Civil and Environmental Engineering, Colorado State University, Fort Collins, CO 80525, USA*

Abstract. In the present study, a new assessment simulation of ride safety based on a new wind-traffic-pavement-bridge coupled vibration system is developed considering stochastic characteristics of traffic flow and bridge surface. Compared to existing simulation models, the new assessment simulation focuses on introducing the more realistic three-dimensional vehicle model, stochastic characteristics of traffic, vehicle accident criteria, and bridge surface conditions. A three-dimensional vehicle model with 24 degrees-of-freedoms (DOFs) is presented. A cellular automaton (CA) model and the surface roughness are introduced. The bridge deck pavement is modeled as a boundless Euler-Bernoulli beam supported on the Kelvin model. The wind-traffic-pavement-bridge coupled equations are established by combining the equations of both the vehicles in traffic, pavement, and bridge using the displacement and interaction force relationship at the patch contact. The numerical simulation shows that the proposed method can simulate rationally useful assessment and prevention information for traffic, and define appropriate safe driving speed limits for vulnerable vehicles under normal traffic and bridge surface conditions.

Keywords: bridge; traffic; vibration; ride safety; bridge surface

1. Introduction

In most countries, road accidents are usually causing more injuries and casualties than any other natural or man-made hazard. Among various causes of crashes, excessive speeds and adverse environments were found as the two dominant causes to the road accidents (Chen and Feng 2010). In addition to direct safety threats, frequent vehicle accidents will also cause serious congestions of the whole highway network in normal situations. Therefore, it is critical to accurately predict the crash risk and further advise appropriate driving speeds under complicated adverse driving environments. Ride safety of the moving vehicles have been caught much attention by the researchers, especially for the situation of the vehicles moving on long-span bridges in windy environments (Xu and Guo 2004, Chen and Cai 2004, Yin *et al.* 2011, Cai *et al.* 2015).

In most existing studies, significant efforts have been given on simulating vehicle dynamics

---

and accidents with engineering simulation models, from the simple rigid body model to the complicated spring-mass multiple-degree of freedom model (Clough and Penzien 1993, Deng and Wang 2014, Han *et al*. 2015). However, extensive works on vehicle accident risks, which considers the coupling among the more realistic three-dimensional vehicle model, stochastic characteristics of traffic, vehicle accident criteria, and bridge surface conditions, is still very limited. To study the ride safety based on wind-bridge-vehicle coupled interaction, either simplified the stochastic traffic flow with multiple vehicles distributed with assumed patterns (Chen and Cai 2007) or modeled the traffic flow as a simplified statistical process (Chen and Feng 2006). Recently, the stochastic characteristics of traffic flows were studied and significant effect was found on the dynamic performance of long-span bridges (Chen and Wu 2010, Deng *et al*. 2014, Liu *et al*. 2016). However, the contribution of pavement response was still not considered in these studies. For example, the pavement was simplified as a rigid base and the deformation of pavement was ignored (Chen and Wu 2010, Yin *et al*. 2011, Yin *et al*. 2016, Han *et al*. 2016). In reality, when a vehicle travelling on the pavement, the wheel forces are generated and applied to the pavement, which in turn induces an increment in pavement response and affects the amount of distress produced by the vehicle.

This paper presents a new assessment simulation of ride safety based on a new wind-traffic-pavement-bridge coupled vibration system. Compared to existing simulation models, the new coupled system focuses on introducing the more realistic three-dimensional vehicle model, pavement simulation, stochastic characteristics of traffic, vehicle accident criteria, and bridge surface roughness. A three-dimensional vehicle model with 24 degrees-of-freedoms (DOFs) is presented. A cellular automaton (CA) model and the bridge surface roughness are introduced. The bridge deck pavement was modeled as a boundless Euler-Bernoulli beam supported on the Kelvin model. The wind-traffic-pavement-bridge coupled equations are established by combining the equations of motion of both the vehicles in traffic, pavement, and bridge using the displacement and interaction force relationship at the patch contact. The numerical simulations show that the proposed method can simulate rationally provide useful assessment information for traffic, and define appropriate safe driving speed limits for vulnerable vehicles under normal and busy traffic conditions.

2. Method of wind-traffic-pavement-bridge interaction analysis

2.1 Equations of motion for a three dimensional wind-traffic-pavement-bridge vibration system

Based on the vehicle model of 12 degrees-of-freedoms (DOFs) in Yin *et al*. (2011), in the present study, a new full-scale vehicle model with 24 degrees-of-freedoms (DOFs) was developed including a three-dimensional driver seat model and the longitudinal vibration of the vehicle (Figs. 1 and 2) (Liu *et al*. 2016, Yin *et al*. 2016). The total DOFs include the longitudinal displacements (x_t), vertical displacements (z_t), lateral displacements (y_t), pitching rotations (θ_t), roll displacements (ϕ_t), and yawing angle (φ_t) of the vehicle truck body, and the longitudinal displacement (x_{al}^1, x_{ar}^1, x_{al}^2, and x_{ar}^2), vertical displacements (z_{al}^1, z_{ar}^1, z_{al}^2, and z_{ar}^2) and lateral displacements (y_{al}^1, y_{ar}^1, y_{al}^2, and y_{ar}^2) of the vehicle's first to second axles; and $z_{su}(x_{su}, y_{su})$ and $z_{ss}(x_{ss}, y_{ss})$ represent the vertical(longitudinal, lateral) displacement of the occupant mass m_{su} and suspension seat mass m_{ss}

of the driver seat, respectively. In the subscripts, the "*t*" and "*a*" represent the truck and axle suspensions, respectively; "*l*" and "*r*" represent the left and right on the axles, respectively; and "*su*" and "*ss*" represent the occupant mass and suspension seat, respectively.

The equation of motion of the vehicle model can be written as (Liu et *al*. 2016, Yin *et al*. 2016)

$$\left[M_v\right]\left\{\ddot{U}_v\right\}+\left[C_v\right]\left\{\dot{U}_v\right\}+\left[K_v\right]\left\{U_v\right\}=\left\{F_G\right\}+\left\{F_{v\text{-}p}\right\}+\left\{F_{vw}\right\} \tag{1}$$

where $\left[M_v\right]$, $\left[C_v\right]$, and $\left[K_v\right]$ = the mass, damping, and stiffness matrices of the vehicle, respectively; $\left\{U_v\right\}$ = the vector including the displacements of the vehicle; $\left\{F_G\right\}$ = gravity force vector of the vehicle; and $\left\{F_{v\text{-}p}\right\}$ = vector of the wheel-pavement contact forces acting on the vehicle; and $\left\{F_{vw}\right\}$ = vector of the wind forces acting on the vehicle.

2.2 Equations of motion for pavement and bridge models

Based on the pavement studies (Mamlouk 1997, Andersen *et al*. 2001, Cao *et al*. 2011), the pavement can be modeled as an Euler-Bernoulli beam supported on the Kelvin model, as shown in Fig. 3.
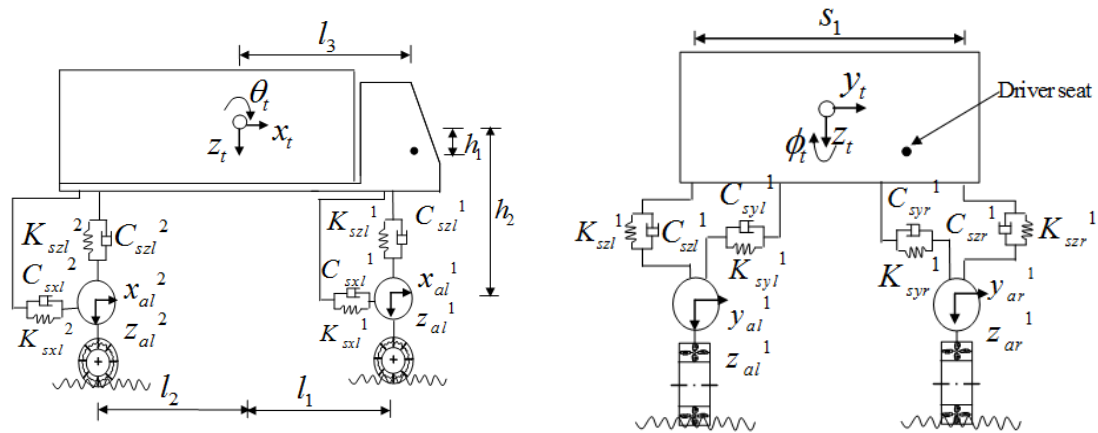

Fig. 1 A new full-scale vehicle model
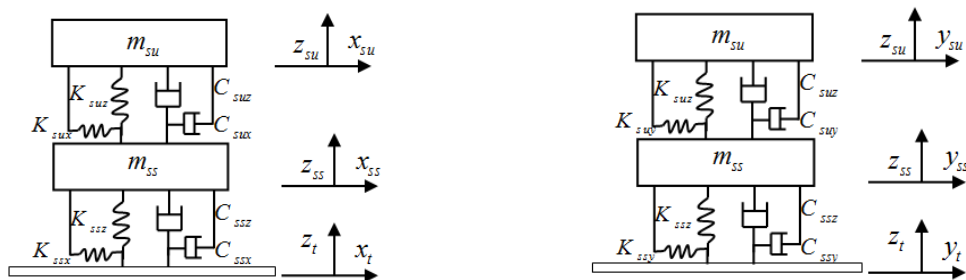
Fig. 2 A three-dimensional driver seat model
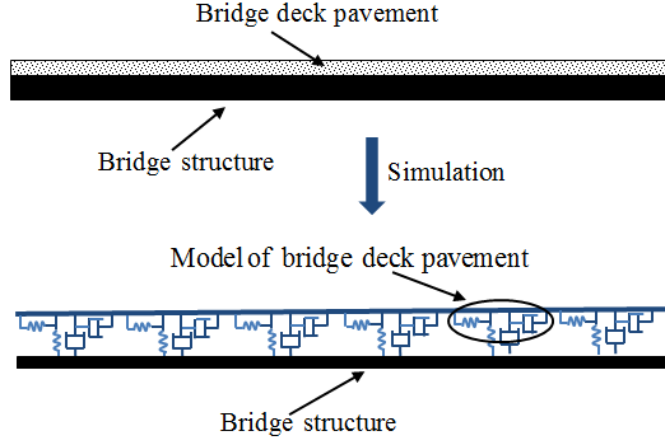
Fig. 3 Pavement model

The equation of motion of a pavement model can be written as

$$E_p I_p y_p''' + m_p \ddot{y}_p + c_p \dot{y}_p = \left(F_G + F_{v\text{-}b}\right)\delta(x - vt) - K_k(y_p - y_b) - C_k(\dot{y}_p - \dot{y}_b) \quad (2)$$

or

$$[\mathbf{M_P}]\{\ddot{U}_P\} + [\mathbf{C_P}]\{\dot{U}_P\} + [\mathbf{K_P}]\{U_P\} = \{\mathbf{F_{p\text{-}v}}\} - \{\mathbf{F_{P\text{-}b}}\} \quad (3)$$

where $\left[\mathbf{M_p}\right]$, $\left[\mathbf{C_p}\right]$, and $\left[\mathbf{K_p}\right]$ are the mass, damping, and stiffness matrices of the pavement, respectively; $\{\mathbf{U_p}\}$ is the displacement vector for all DOFs of the pavement; $\{\dot{\mathbf{U}}_\mathbf{p}\}$ and $\{\ddot{\mathbf{U}}_\mathbf{p}\}$ are the first and second derivative of $\{\mathbf{U_p}\}$ with respect to time, respectively; and $\{\mathbf{F_{p\text{-}v}}\}$ is a vector containing all external forces acting on the pavement; $\{\mathbf{F_{p\text{-}b}}\}$ is a vector containing interaction forces between bridge and pavement.

The equation of motion of a bridge structural model can be written as

$$E_b I_b y_b''' + m_b \ddot{y}_b + c_b \dot{y}_b = K_k(y_p - y_b) + C_k(\dot{y}_p - \dot{y}_b) \quad (4)$$

or

$$[\mathbf{M_b}]\{\ddot{U}_b\} + [\mathbf{C_b}]\{\dot{U}_b\} + [\mathbf{K_b}]\{U_b\} = \{\mathbf{F_{b\text{-}p}}\} \quad (5)$$

where $\left[\mathbf{M_b}\right]$, $\left[\mathbf{C_b}\right]$, and $\left[\mathbf{K_b}\right]$ are the mass, damping, and stiffness matrices of the bridge, respectively; $\{\mathbf{U_b}\}$ is the displacement vector for all DOFs of the bridge; $\{\dot{\mathbf{U}}_\mathbf{b}\}$ and $\{\ddot{\mathbf{U}}_\mathbf{b}\}$ are the first and second derivative of $\{\mathbf{U_b}\}$ with respect to time, respectively; and $\{\mathbf{F_{b\text{-}p}}\}$ is a vector containing interaction forces between bridge and pavement.

2.3 Simplified quasi-steady wind forces on a three-dimensional vehicle model

Wind action on a running vehicle includes static and dynamic load effects. The quasi static wind forces on vehicles are adopted (Baker 1991, Chen and Cai 2004)

$$F_{xw} = \frac{1}{2}\rho_\alpha A U_R^2 C_D(\psi); \quad F_{zw} = \frac{1}{2}\rho_\alpha A U_R^2 C_L(\psi); \quad F_{yw} = \frac{1}{2}\rho_\alpha A U_R^2 C_S(\psi);$$

$$M_{xw} = \frac{1}{2}\rho_\alpha A h_v U_R^2 C_R(\psi); M_{yw} = \frac{1}{2}\rho_\alpha A h_v U_R^2 C_P(\psi); M_{zw} = \frac{1}{2}\rho_\alpha A h_v U_R^2 C_Y(\psi) \quad (6)$$

where F_{xw}, F_{yw}, F_{zw}, M_{xw}, M_{yw} and M_{zw} are the drag force, side force, lift force, rolling moment, pitching moment and yawing moment acting on the vehicle, respectively. ρ_α is the are density. C_D, C_S, C_L, C_R, C_P and C_Y are the coefficients of drag force, side force, lift force, rolling moment, pitching moment and yawing moment for the vehicle, respectively. "A" is the frontal area of the vehicle; h_v is the distance from the gravity center of the vehicle to the bridge surface; and U_R is the relative wind speed to the vehicle, which is defined as

$$U_R^2 = [(U + u(x,t))\cos\beta + \dot{S}]^2 + [(U + u(x,t))\sin\beta]^2$$

$$\tan\psi = \frac{(U + u(x,t))\sin\beta}{(U + u(x,t))\cos\beta + \dot{S}} \quad (7)$$

where $\dot{S}$ is the driving speed of vehicle; U and $u(x, t)$ are the mean wind speed and turbulent wind speed component on the vehicle, respectively; β is the attack angle of the wind to the vehicle, which is the angle between the wind direction and the vehicle moving direction; and ψ is usually between 0 to π.

2.4 Wind forces on bridge in modal coordinates

The dynamic model of long-span bridges can be obtained through finite element method using different kinds of finite elements such as beam elements and truss elements. With the obtained mode shapes, the response corresponding to any point along the bridge deck can be evaluated in the time domain. The structural nonlinearity is typically considered in the static analysis before a dynamic analysis is conducted. Equations of motions in the three directions including vertical, lateral, and torsion of the bridge with the mode superposition technique a can be obtained and can be rewritten in a matrix form as (Clough and Penzien 1993, Chen and Cai 2004)

$$[M_b]\{\ddot{U}_b\} + [C_b]\{\dot{U}_b\} + [K_b]\{U_b\} = \{F_{bw}\} \quad (8)$$

where $[M_b]$, $[C_b]$, and $[K_b]$ are the mass, damping, and stiffness matrices of the bridge, respectively; $\{U_b\}$ is the displacement vector for all DOFs of the bridge; $\{\dot{U}_b\}$ and $\{\ddot{U}_b\}$ are

the first and second derivative of $\{U_b\}$ with respect to time, respectively; and $\{F_{bw}\}$ is the vector of the wind forces acting on the bridge.

2.5 Assembling the vehicle-pavement-bridge coupled system

Vehicles traveling on the pavement are connected to the pavement via patch contacts. The interaction forces acting on the pavement $\{F_{p-v}\}$ and the interaction forces acting on the vehicles $\{F_{v-p}\}$ are actually a pair of action and reaction forces existing at the patch contacts. In terms of finite element modeling, these interaction forces may not be applied right at any nodes. Therefore, the interaction forces need to be transformed into equivalent nodal forces $\{F_b{}^{eq}\}$ in the finite element analysis. This can be done using the virtual work principle, which states that the work done by the equivalent nodal forces and the actual force should be equal. Thus, it can be expressed as

$$\{y_{p\_nodal}\}^T \{F^{eq}\} = y_{px\_contact} \cdot F \tag{9}$$

where $\{y_{p\_nodal}\}$ is the displacement vector for all the nodes of the element in contact; $y_{px\_contact}$ is the displacement of the element bearing the tire spring load at the contact position x; $\{F^{eq}\}$ is the equivalent force vector applied at all the nodes of the element in contact; and F is the real force acting at the patch contact.

The $y_{px\_contact}$ can be expressed using the displacement at each node of the element as

$$y_{px\_contact} = [N_e]\{y_{p\_nodal}\} \tag{10}$$

where $[N_e]$ is the relationship function of the element in contact. From Eqs. (9) and (10), the relationship between the equivalent nodal forces and the interaction force acting on the element in contact is expressed as

$$\{F^{eq}\} = [N_e]^T \cdot F \tag{11}$$

To be consistent with the size of the force vector $\{F_p{}^{eq}\}$ in the analysis of the full pavement, Eq. (11) can be expanded to a full force vector form as

$$\{F_p{}^{eq}\} = [N_p]^T \cdot F \tag{12}$$

where $\{F_p{}^{eq}\}$ is a vector with the number of elements equal to the total number of DOFs of the pavement. It should be noted that, for two interaction forces acting upon different elements of the same pavement, the relationship function of the pavement $[N_p]$ for the two forces would be different though the element relationship function $[N_e]$ may be the same, because the corresponding DOFs of the non-zero terms in the two force vectors are different.

In a pavement-vehicle system, the relationship among the vertical displacement of vehicle body $y_v{}^i$, pavement deflection at the contact position $y^i_{px\_contact}$, the radial deformation of ith tire spring $U_{tyx}{}^i$ at the position x, and road surface profile $r(x)^i$, can be rewritten as

$$U_{tyx}{}^i = \{y_v{}^i - [-r(x)^i] - y^i_{px\_contact}\}/\cos\theta$$

$$y_v{}^i = y_a{}^j \pm (s_j/2)\phi_a{}^j + \Delta^i - R(1-\cos\theta), \quad j=1,2$$

(13)

The first derivative of Eq. (13) can then be obtained as

$$\dot{U}_{tyx}{}^i = (\dot{y}_v^i + \dot{r}(x)^i - \dot{y}^i_{px\_contzct})/\cos\theta$$

(14)

where $\dot{y}_v^i$ is the velocity of the vehicle body in the vertical direction; $\dot{r}(x)^i = \dfrac{dr(x)^i}{dx}\dfrac{dx}{dt} = \dfrac{dr(x)^i}{dx}v(t)$, where $v(t)$ is the vehicle traveling velocity; and $y^i_{px\_contact}$, according to the definition of the relationship function of the pavement in Eq. (10), can be expressed as

$$y^i_{px\_contact} = [N_e]\cdot\left\{y^i_{p\_nodal}\right\} = [N_p]\cdot\left\{y_p\right\}$$

(15)

The interaction force acting on the ith tire can be obtained as

$$F^i_{v-p} = -F^i_{ty} - F^i_{dty}$$
$$= -\int_{x^i-l_{ty}/2}^{x^i+l_{ty}/2}k_{ty}^i(y_v^i + r(x)^i - [N_p^i]\{y_p\})dx - \int_{x^i-l_{ty}/2}^{x^i+l_{ty}/2}c_{ty}^i\left(\dot{y}_v^i - \frac{d[N_p^i]}{dx}v^i(t)\{y_p\} - [N_p^i]\{\dot{y}_p\} + \frac{dr(x)^i}{dx}v^i(t)\right)dx$$

(16)

Compared the length of l_{ty} with the total length of the bridge, the l_{ty} is small. Therefore, the value of y_p and y_v can be assumed as a constant in the length range form $x^i - l_{ty}/2$ to $x^i + l_{ty}/2$. Eq. (16) can be further written as

$$F_{v-p}{}^i = -\int_{x^i-l_{ty}/2}^{x^i+l_{ty}/2}k_{ty}^i\left(y_v^i + r(x)^i - [N_p^i]\{y_p\}\right)dx - \int_{x^i-l_{ty}/2}^{x^i+l_{ty}/2}c_{ty}^i\left(\dot{y}_v^i - \frac{d[N_p^i]}{dx}v^i(x)\{y_p\} - [N_p^i]\{\dot{y}_p\} + \frac{dr(x)^i}{dx}v^i(t)\right)dx$$

$$= -\int_{x^i-l_{ty}/2}^{x^i+l_{ty}/2}k_{ty}^i dxy_v^i - \int_{x^i-l_{ty}/2}^{x^i+l_{ty}/2}k_{ty}^i r(x)^i dx + \int_{x^i-l_{ty}/2}^{x^i+l_{ty}/2}k_{ty}^i[N_p^i]dx\{y_p\} - \int_{x^i-l_{ty}/2}^{x^i+l_{ty}/2}c_{ty}^i dx\dot{y}_v^i + \int_{x^i-l_{ty}/2}^{x^i+l_{ty}/2}c_{ty}^i\frac{d[N_p^i]}{dx}v^i(t)dx\{y_p\}$$

(17)

$$+\int_{x^i-l_{ty}/2}^{x^i+l_{ty}/2}c_{ty}^i[N_p^i]dx\{\dot{y}_p\} - \int_{x^i-l_{ty}/2}^{x^i+l_{ty}/2}c_{ty}^i\frac{dr(x)^i}{dx}v^i(t)dx$$

where $\left[N_p^i\right]$ is the relationship function of the bridge for an interaction force between the ith tire and the pavement.

The *N* interaction forces can be expressed in a vector form as

$$
\begin{aligned}
\{F_{v-p}^{N}\} &= \{F_{v-p}^{1} \quad F_{v-p}^{2} \cdots F_{v-p}^{N}\}^{T} \\
&= -[K_{v-v}^{N}]\{y_v\} - \{F_{v-r}\} + [K_{v-p}]\{y_p\} - [C_{v-v}^{N}]\{\dot{y}_v\} + [K_{v-cp}]\{y_p\} + [C_{v-p}]\{\dot{y}_p\} - \{F_{v-cr}\}
\end{aligned}
\tag{18}
$$

where $\left[K_{v-v}^{\ N}\right]$ and $\left[C_{v-v}^{\ N}\right]$ are the stiffness, and damping matrices for *N* tires, respectively; and $\left[K_{v-p}\right]$, $\{F_{v-r}\}$, $\left[K_{v-cp}\right]$, $\left[C_{v-p}\right]$, and $\{F_{v-cr}\}$ are obtained from Yin *et al*. (2016).

As discussed earlier, the interaction forces acting on the pavement, $\{F_{p-v}\}$, are the reaction forces of that acting on the vehicles, $\{F_{v-p}\}$. Therefore, the following relationship holds

$$
\{F_{p-v}\} = -\{F_{v-p}\}
\tag{19}
$$

Substituting Eqs. (17) and (19) into Eq. (12), the transformed equivalent nodal forces due to the *N* interaction forces can be obtained as

$$
\begin{aligned}
\{F_p^{\ eq}\} &= \sum_{i=1}^{N}[N_p^{\ i}]^T \cdot (-F_{v-p}^{\ i}) \\
&= \sum_{i=1}^{N}[N_p^{\ i}]^T \cdot \left[\begin{matrix} \int_{x^i-l_{ty}/2}^{x^i+l_{ty}/2} k_{ty}^{\ i} dx y_v^{\ i} + \int_{x^i-l_{ty}/2}^{x^i+l_{ty}/2} k_{ty}^{\ i} r(x)^i dx - \int_{x^i-l_{ty}/2}^{x^i+l_{ty}/2} k_{ty}^{\ i}[N_p^{\ i}] dx \{y_p\} + \int_{x^i-l_{ty}/2}^{x^i+l_{ty}/2} c_{ty}^{\ i} dx\, \dot{y}_v^{\ i} \\ -\int_{x^i-l_{ty}/2}^{x^i+l_{ty}/2} c_{ty}^{\ i} \frac{d[N_p^{\ i}]}{dx} v^i(t) dx \{y_p\} - \int_{x^i-l_{ty}/2}^{x^i+l_{ty}/2} c_{ty}^{\ i}[N_p^{\ i}] dx \{\dot{y}_p\} + \int_{x^i-l_{ty}/2}^{x^i+l_{ty}/2} c_{ty}^{\ i} \frac{dr(x)^i}{dx} v^i(t) dx \end{matrix} \right] \\
&= [K_{p-v}]\{y_v\} + \{F_{p-r}\} - [K_{p-vp}]\{y_p\} + [C_{p-v}]\{\dot{y}_v\} - [K_{p-cp}]\{y_p\} - [C_{p-p}]\{\dot{y}_p\} + \{F_{p-cr}\}
\end{aligned}
\tag{20}
$$

where $\left[K_{p-v}\right]$, $\left[K_{p-vp}\right]$, $\{F_{p-r}\}$, $\left[C_{p-v}\right]$, $\left[K_{p-cp}\right]$, $\left[C_{p-p}\right]$, and $\{F_{p-cr}\}$ are obtained from Yin *et al*. (2016).

The interaction forces acting on the bridge, $\{F_{p-b}\}$, are the reaction forces of that acting on the pavement, $\{F_{b-p}\}$.

Substituting Eq. (18) into Eq. (3)

$$
\begin{aligned}
[M_v^{N}]\{\ddot{y}_v\} + [C_v^{N}]\{\dot{y}_v\} + [K_v^{N}]\{y_v\} &= F_G^{N} - [K_{v-v}^{N}]\{y_v\} + \\
[K_{v-p}]\{y_p\} - \{F_{v-r}\} - [C_{v-v}^{N}]\{\dot{y}_v\} + [K_{v-cp}]\{y_p\} &+ [C_{v-p}]\{\dot{y}_p\} - \{F_{v-cr}\}
\end{aligned}
\tag{21}
$$

Since $\{F_p^{\ eq}\}$ in Eq. (19) is actually the equivalent force vector of the external force vector $\{F_{p-v}\}$ in Eq. (3), after substituting Eq. (19) into Eq. (3), the following can be obtained

$$\left[M_p\right]\{\ddot{y}_p\}+\left[C_p\right]\{\dot{y}_p\}+\left[K_p\right]\{y_p\}=\left[K_{p-v}\right]\{y_v\}-\left[K_{p-vp}\right]\{y_p\}+\{F_{p-r}\}+\left[C_{p-v}\right]\{\dot{y}_v\}-$$
$$\left[K_{p-cp}\right]\{y_p\}-\left[C_{p-p}\right]\{\dot{y}_p\}+\{F_{p-cr}\}-[K_{b-p}]\{y_p\}+[K_{p-b}]\{y_b\}-[C_{b-p}]\{\dot{y}_p\}+[C_{p-b}]\{\dot{y}_b\} \quad (22)$$

The equation of motion of a bridge structural model can be written as

$$[M_b]\{\ddot{y}_b\}+[C_b]\{\dot{y}_b\}+[K_b]\{y_b\}=[K_{b-p}]\{y_p\}-[K_{p-b}]\{y_b\}+[C_{b-p}]\{\dot{y}_p\}-[C_{p-b}]\{\dot{y}_b\} \quad (23)$$

3. Equations of motion for wind-traffic-pavement-bridge vibration system

3.1 Traffic flow simulation

The traffic simulation using the CA traffic model can capture the basic features of the probabilistic traffic flow by adopting the realistic traffic rules such as car-following and lane-changing, as well as actual speed limits. One of the most important CA models is NaSch model (Nagel and Schreckenberg 1992). Though NaSch model is simple, it can describe some traffic phenomena in reality, such as phase transition etc. In recent years, the CA traffic model was introduced and verified to study the vibration of bridges under the traffic flow (Chen and Wu 2010). However, all those aforementioned CA models above do not take into account the influence of the next-nearest neighbor vehicles, though this influence exists in real traffic and cannot be ignored (Kong *et al*. 2006). In this paper, an improved CA model considering the influence of the next-nearest neighbor vehicles in Kong *et al.* (2006) is introduced and used to simulate the traffic flow.

In the car-following model, most researchers usually consider the influence of the vehicle ahead using the following equation (Kong *et al.* 2006)

$$\ddot{x}_n(t+T)=\lambda(\dot{x}_{n+1}-\dot{x}_n) \quad (24)$$

where T is a response time lag, λ is the sensitivity coefficient, $\ddot{x}_n$ is the acceleration of the nth vehicle, and $\dot{x}_n$ is the velocity of the *nth* vehicle , $\dot{x}_{n+1}$ is the velocity of the *(n+1)th* vehicle. The model shows that the response of the following vehicle is in direct proportion to the stimulus received from the leading vehicle. Considering the influence of the next-nearest neighbor vehicles, the Eq. (24) can be changed to

$$\ddot{x}_n=\lambda_1(\dot{x}_{n+1}-\dot{x}_n)_{t-T_1}+\lambda_2(\dot{x}_{n+2}-\dot{x}_n)_{t-T_2} \quad (25)$$

where T_1 is a response time lag of the nearest neighbor ahead, T_2 is a response time lag of the next-nearest neighbor ahead, λ_1 and λ_2 are the sensitivity coefficients of the nearest neighbor and next nearest neighbor vehicles, respectively, and both of them are confined between 0 and 1. Driving strategies are based on the double-look-ahead model for the acceleration step in the NaSch model. According to Eq. (25), suppose $\lambda_1>\lambda_2$, the acceleration of the vehicle is written as

$$\ddot{x}_n(t+1)=\lambda(\Delta\dot{x}_{n+1}(t),\Delta\dot{x}_{n+2}(t-1)) \quad (26)$$

where $\dot{\lambda} = \lambda_1(\dot{x}_{n+1}(t) - \dot{x}_n(t)) + \lambda_2(\dot{x}_{n+2}(t-1) - \dot{x}_n(t-1))$. Using Eq. (26), the rule of the acceleration /deceleration can be changed in the NaSch model.

5. Equations of motion for traffic flow-pavement-bridge-wind vibration system

In the present study, the vehicle is modeled with 24 DOFs of the three dimensional vehicle models, light truck is used with the single DOF of vehicle model to be computationally efficient.

The 24 DOFs and single DOF vehicle models are shown in Figs. 1 and 2, respectively. Using the displacement relationship and the interaction force relationship at the contact patches, the vehicle-bridge coupled system can be established by combining the equations of motion of both the bridge and vehicles. Eqs. (21), (22), and (23) can be combined and rewritten in a matrix form as

$$
\begin{bmatrix} \mathbf{M_b} & & \\ & \mathbf{M_p} & \\ & & \mathbf{M_v^N} \end{bmatrix} \begin{Bmatrix} \ddot{\mathbf{Y}}_b \\ \ddot{\mathbf{Y}}_p \\ \ddot{\mathbf{Y}}_v \end{Bmatrix} + \begin{bmatrix} \mathbf{C_b + C_{p-b}} & -\mathbf{C_{b-p}} & \\ -\mathbf{C_{p-b}} & \mathbf{C_p + C_{p-p}} & -\mathbf{C_{p-v}^N} \\ & -\mathbf{C_{v-p}^N} & \mathbf{C_v^N + C_{v-v}^N} \end{bmatrix} \begin{Bmatrix} \dot{\mathbf{Y}}_b \\ \dot{\mathbf{Y}}_p \\ \dot{\mathbf{Y}}_v \end{Bmatrix} +
$$

$$
\begin{bmatrix} \mathbf{K_b + K_{p-b}} & -\mathbf{K_{b-p}} & \\ -\mathbf{K_{p-b}} & \mathbf{K_p + K_{p-vp}^N + K_{p-cp}^N + K_{b-p}} & -\mathbf{K_{p-v}^N} \\ & -\mathbf{K_{v-p}^N - K_{v-cp}^N} & \mathbf{K_v^N + K_{v-v}^N} \end{bmatrix} \begin{Bmatrix} \mathbf{Y_b} \\ \mathbf{Y_p} \\ \mathbf{Y_v} \end{Bmatrix} = \begin{Bmatrix} \mathbf{F_{bw}^N} \\ \mathbf{F_{p-r}^N + F_{p-cr}^N} \\ -\mathbf{F_{v-r}^N - F_{v-cr}^N + F_G^N + F_{vw}^N} \end{Bmatrix} \quad (27)
$$

where $\mathbf{N}$ is the number of vehicles traveling on the bridge, $\mathbf{M_v^N}, \mathbf{C_v^N}$, and $\mathbf{K_v^N}$ are mass, damping, and stiffness matrices for the vehicle, respectively; $\mathbf{C_{b-vb}^N}$ and $\mathbf{K_{b-vb}^N}$ are damping and stiffness contribution to the bridge structure due to the coupling effects between the N vehicles in the vehicle and the bridge system, respectively; $\mathbf{C_{b-v}^N}$ and $\mathbf{K_{b-v}^N}$ are the coupled stiffness and damping matrices contributing to bridge vibration from the N vehicles in the vehicles, respectively; $\mathbf{C_{v-b}^N}$ and $\mathbf{K_{v-b}^N}$ are the coupled damping and stiffness matrices contributing to the vibration of the N vehicles, respectively; $\mathbf{C_{v-v}^N}$ and $\mathbf{K_{v-v}^N}$ are the coupled damping and stiffness matrices of induced by other vehicles in the vehicles, respectively. Eq. (27) can be solved by the *New-mark* method in the time domain.

As discussed by Chen and Cai (2007), the traffic flow-pavement-bridge-wind coupled Eq. (27) can consider various types and numbers of vehicles at any location on the bridge. When the real traffic flow is simulated, the dynamic model of each vehicle will be substituted into Eq. (27) for a "fully coupled" traffic flow-pavement-bridge-wind dynamic interaction analysis. In order to simplify the vehicle models in traffic, all the vehicles are classified as three types: (1) v1-heavy multi-axle trucks; (2) v2-light trucks and buses; and (3) v3-sedan car. Only heavy trucks are modeled with 24 DOFs of the three dimensional vehicle models, light trucks and sedan cars are

used with the single DOF of vehicle model to be computationally efficient. Mechanical and geometric properties can be obtained from Yin *et al.* (2011) and Chen and Cai (2007).

6. Criteria of wheel being lifted up or sideslip

6.1 Lifted up

As in Chen and Chen (2010), when the weight transferred between the left and right wheels is larger than a half of the vehicle weight minus a half of the vertical wind force, lift force, there is no reaction force existing on one side of wheels. In addition, the roll angle between the sprung mass and the suspension system typically cannot exceed 6° or 7° due to the mechanical restraints of the suspension movements (Chen and Chen 2010). Thus if either of the following two criteria is satisfied, the wheel is believed to be lifted up.

$$W_{trans} > M_V g / 2 - F_{W,Z} / 2 \tag{28}$$

or

$$\phi_t - \phi_{t,f} \geq \phi^{cri} \quad or \quad \phi_t - \phi_{t,r} \geq \phi^{cri} \tag{29}$$

where ϕ_t and $\phi^i_{t,f}$ are absolute roll angle of sprung mass and un-sprung mass, respectively; ϕ^{cri} is maximum allowable relative roll-over angle due to the mechanical restraints (e.g., 7°);

W_{trans} =the weight transfer ratio between the left and right wheels, $\dot{\beta}$ and $\dot{\psi}$ =sideslip angle and heading angle; and *u*=active roll torque.

6.2 Sideslip

According to Gim and Nikravesh (1990), the lateral force of a pneumatic tire-bridge surface interaction can be considered as a resultant force composed of three components of force F_{ys}, $F_{y\alpha}$, and $F_{y\gamma}$ due to the tire running with an "S" shape, slip angle α, and camber angle γ, respectively. The lateral force can be obtained as (See more description and definition in Gim and Nikravesh (1990))

$$F_y = F_{y\alpha} + F_{y\gamma} + F \tag{30}$$

$$F_{y\alpha} = -\text{sign}(\alpha) \cdot [C_\alpha S_\alpha l_n^2 + \left(\mu_y - \frac{C_\gamma S_\gamma}{F_{v-b}} \right) F_z (1 - 3l_n^2 + 2l_n^3)] \tag{30a}$$

$$F_{y\gamma} = -\text{sign}(\gamma) \cdot C_\gamma S_\gamma \tag{30b}$$

$$F_{ys} = [k_{ty}(y_a^i + y_{ts} - y^i_{bx\_contact}) + c_{ty}(\dot{y}_a^i + \dot{y}_{ts} - \dot{y}^i_{bx\_contact})] l_{tr} \tag{30c}$$

where C_α is the cornering stiffness; S_α is the absolute value of the lateral slip ratio S_{sy}; a

non-dimensional contact patch length l_n is defined as $l_n = l_\alpha / l_{ty}$, where l_α is the length of the adhesion region from the front extremity to the breakaway point for the sliding region of the contact patch, therefore, l_α is varied from 0 to the value of l_{ty} is the patch length of the wheel; μ_y is the tire-bridge surface friction coefficient in the slipping region; F_z is the tire vertical force acting on the bridge surface and equals $-F_{v-b}$; C_γ is the camber stiffness; and S_γ is the absolute value of the lateral slip ratio due to the camber angle γ and defined as: $S_\gamma = \left| \sin \gamma \right|$. Based on the studies in Gim and Nikravesh (1990) and Yin *et al*. (2011), the slip angle can be varied from -10° to 10°, and the camber angle varies from -8° to 8°. Furthermore, k_{ty} and c_{ty} are the tire lateral stiffness and damping coefficients per unit length of the wheel; $y_a{}^i$ is the lateral displacement of the vehicle axle; y_{ts} is the tire lateral displacement due to tire running with an "S" shape ; and $y^i{}_{bx\_contact}$ is the bridge dynamic lateral deflection at the contact position x .

The problem of simulating the tire running with an "S" shape is very complex. In this study, to simplify the model, the "S" shape was assumed as a "Sine" shape with a random amplitude and random phase angle, similar to the assumptions made in Fujii and Yoshimoto (1975) and Fujii *et al*. (1975). As a result, y_{ts} can be expressed as

$$y_{ts}(x) = A_s \sin(\frac{2\pi x}{l_s} + \varphi_s)$$

(31)

where A_s is the random amplitude; l_s is the wavelength; and φ_s is the initial phase angle. Based on the studies (Fujii and Yoshimoto 1975, Fujii *et al*. 1975), A_s can be assumed to follow a symmetrical distribution from 2.5 mm to 5 mm; l_s can be obtained from a symmetrical distribution from 6.65 m to 10 m; and φ_s can also be assumed to follow a symmetrical distribution from 0 to 2π (Fujii and Yoshimoto 1975). The front or the rear wheel will start to sideslip when the actual lateral tire forces F_y, quantified with Eq. (3) exceeds the corresponding sideslip critical friction forces.

$$F_y > \mu F_z$$

(32)

where μ is static lateral friction coefficient; F_z is vertical reaction force on the axle.

6.3 Critical driving speed and critical sustained time

Critical driving speed (CDS) is the highest allowable driving speed without causing any type of accidents under a specific combination of environmental and vehicle conditions. Some researchers studied using different vehicle models in some existing studies (Baker 1991, Chen and Cai 2004, Guo and Xu 2006, Chen and Chen 2010); another critical variable which was discussed by Chen and Chen (2010) is the "critical sustained time (CST)." CST is the minimum time period required to sustain the specific combination of the adverse environments e.g., wind speed and the driving

conditions e.g., specific driving speed.

According to the Green book (AASHTO 2004), the median reaction time of drivers is 0.66 s based on the data from 321 drivers. In the present study, the "median reaction time" 0.66 s will be used. If the CST is larger than the reaction time of the driver, the driver may have sufficient time to take appropriate actions e.g., reduce speeds to possibly prevent the occurrence of accidents. Obviously, CDS suggests the appropriate driving speed assuming the driver has sufficient time to react while CST discloses the information about whether the driver has enough time to react under a particular driving condition.

6.4 Modeling of bridge surface

The bridge surface profile is assumed usually to be a zero-mean stationary Gaussian random process and can be generated through an inverse Fourier transformation based on a power spectral density (PSD) function (Yin *et al*. 2011) as

$$r^i(x) = \sum_{k=1}^{N} \sqrt{2\varphi(n_k)\Delta n} \cos(2\pi n_k x + \theta_k) \tag{33}$$

where θ_k is the random phase angle uniformly distributed from 0 to 2π; $\varphi()$ is the PSD function (m^3/cycle) for the bridge surface elevation; and n_k is the spatial frequency (cycle/m). In the present study, the following PSD function (Yin *et al*. 2011) was used

$$\varphi(n) = \varphi(n_0)(\frac{n}{n_0})^{-2} \qquad (n_1 < n < n_2) \tag{34}$$

where n is the spatial frequency (cycle/m); n_0 is the discontinuity frequency of $1/2\pi$ (cycle/m); $\varphi(n_0)$ is the roughness coefficient (m^3/cycle) whose value is chosen depending on the bridge condition; and n_1 and n_2 are the lower and upper cut-off frequencies, respectively. The International Organization for Standardization (ISO) (1995) has proposed a bridge roughness classification index from A (very good) to H (very poor) according to different values of $\varphi(n_0)$.

7. Numerical studies

7.1 Description of the cable-stayed bridge

As a prototype bridge used in the present study, the Jinyu Highway Bridge, located at the border of Hunan province in China, is an unsymmetrical hybrid cable-stayed bridge with a box section, double towers, double cable planes, and with spans of 80 m+208 m+716m+70 m+2x65 m from the north to the south, as shown in Fig. 4. Based on the configuration of the bridge, the bridge girders, tower, and railings were all modeled with solid elements. The cable was modeled with link element, and a rigid connection was assumed between the cable and bridge girders. A rigid connection was also assumed between both girder and diaphragms and between girder and bridge deck. The pavement parameters are: Young's modules E_p=1.5 GPa, thickness h_p=9.5 cm, Poisson's ratio 0.25, and per-unit-length mass m_p=8778 kg/m. A numerical model was created using the FE method with ANSYS software, as seen in Fig. 5.
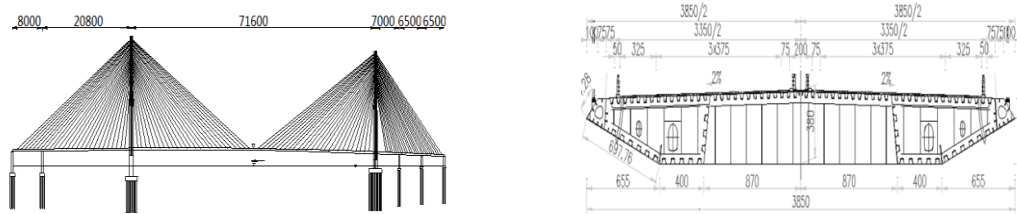
Fig. 4 The Jinyu Highway Bridge (cm)
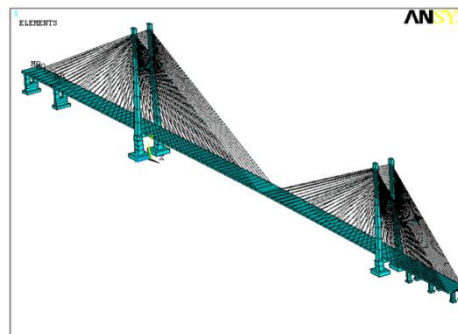
Fig. 5 The full bridge model

7.2 Critical sustained time of accidents

When the truck is driven on a road or bridge with dry road surface, rollover accidents are found in Fig. 6, which shows the relationship between CST of rollover, the wind speed U, and the vehicle speed V. The median reaction time of drivers is 0.66 s based on the data from 321 drivers is a horizontal line shown in the figure. It can be found from Fig. 6 that the CST of rollover decreases when U or V increases, and some CST of rollover are larger than the median reaction time, thus, the accident may not actually happen. For instance, when the wind speed is 50 km/h, the truck and the light truck or sedan moving with a speed of 120 km/h, the truck will take 0.68 s to roll over, and the light truck or sedan will take 1.04 s to roll over. Because the times to roll over are larger than the median reaction time, the accident may not actually happen for the truck and light truck or sedan. When the wind speed is 80 km/h and the truck moves with a speed of 20 km/h, the truck will take 0.61s to roll over, and when the light truck or sedan car moves with a speed of 50 km/h, the light truck or sedan car will take 0.63s to roll over. As compared to the median reaction time (0.66s), the 0.63s and 0.61s are usually too short for most drivers to react and the rollover accidents are very likely to happen. Therefore, the CST of accidents is an important assessment criterion for the ride safety, and the effect of wind speed on the CST of rollover is very significant.

When road surface is covered by snow, Fig. 7 shows the relationship between the CST of sideslip and the driving speed V when the vehicle moves on a snow-covered road surfaces, along with different wind speeds. From the Fig. 7, the sideslip accidents usually happen. It can be found from Fig. 7 that the CST of sideslip decreases when U or V increases. For instance, when the wind speed is 50 km/h, the truck moves with a speed of 50 km/h, the truck will take 0.64 s to sideslip, and the light truck or sedan will take 0.62 s to sideslip with a speed of 70 km/h. As compared to the median reaction time (0.66s), the 0.64s and 0.62 s are usually too short for most drivers to react

(a) Heavy multi-axle truck   (b) Light truck and Sedan car

Fig. 6 CST of rollover accident on the dry surface of bridge

(a) Heavy multi-axle truck   (b) Light truck and Sedan car
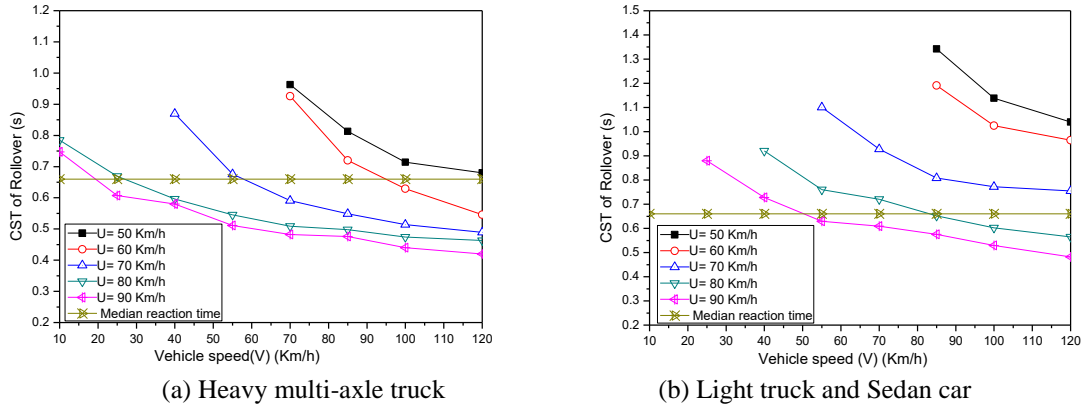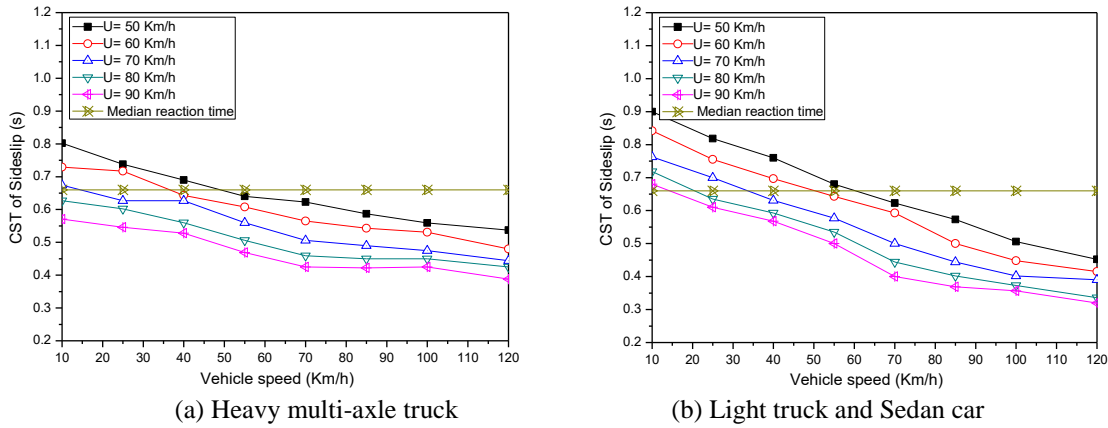
Fig. 7 CST of sideslip accident on the snow-covered surface of bridge

and the sideslip accidents are very likely to happen. Therefore, the effect of the CST of sideslip on the accident is very significant.

7.3 Critical driving speeds of accidents

As the simulation of the Figs. 6 and 7, based on the CST of the results, Figs. 8 and 9 show the CDS of the truck, light truck and sedan car under different wind conditions on surface of bridge and snow-covered surface of bridge. Fig. 8 shows the CDS of rollover accident on the dry surface of bridge, and Fig. 9 shows the CDS of sideslip accident on the snow-covered surface of bridge.

It can be found from Fig. 8(a) that a rollover accident will not occur when the wind speed does not exceed 50 km/h. When the wind speed is more than 90 km/h and even the truck moves with V=10 km/h, it will have the risk of being blown over. Compared to the truck, the rollover possibility of light truck and sedan car is much littler than that of the truck. From Fig. 8(b), it can be found that when the wind speed does not exceed 70km/h, a rollover accident will not occur. When the wind speed is 90 km/h, the light truck and sedan car will have the risk of being blown over moving with 50 km/h.
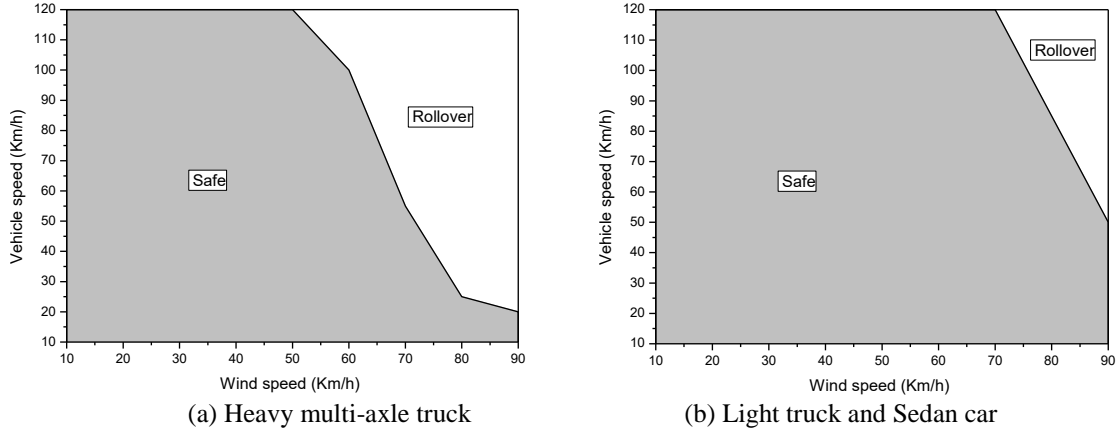
Yin Xinfeng, Liu Yang and Chen S.R

(a) Heavy multi-axle truck

(b) Light truck and Sedan car

Fig. 8 CDS of rollover accident on the dry surface of bridge

(a) Heavy multi-axle truck

(b) Light truck and Sedan car

Fig. 9 CDS of sideslip accident on the snow-covered surface of bridge

(a) Heavy multi-axle truck

(b) Light truck and Sedan car
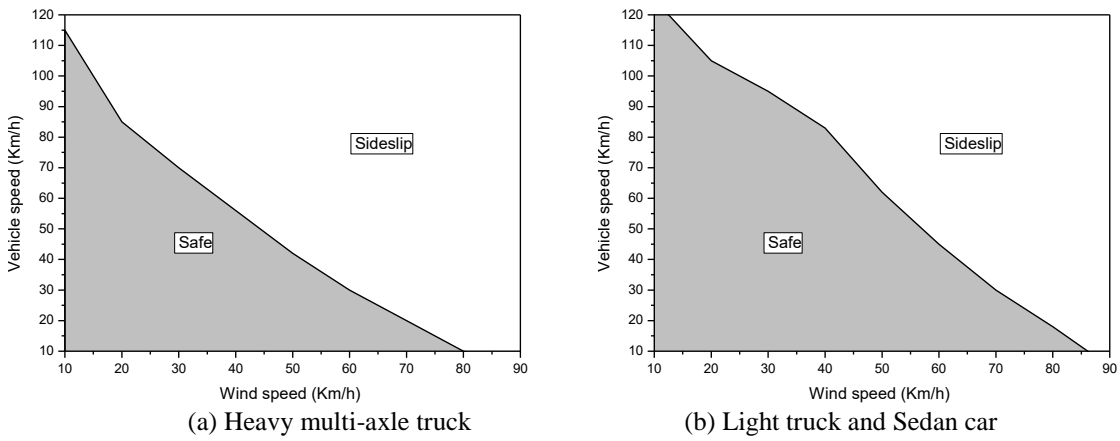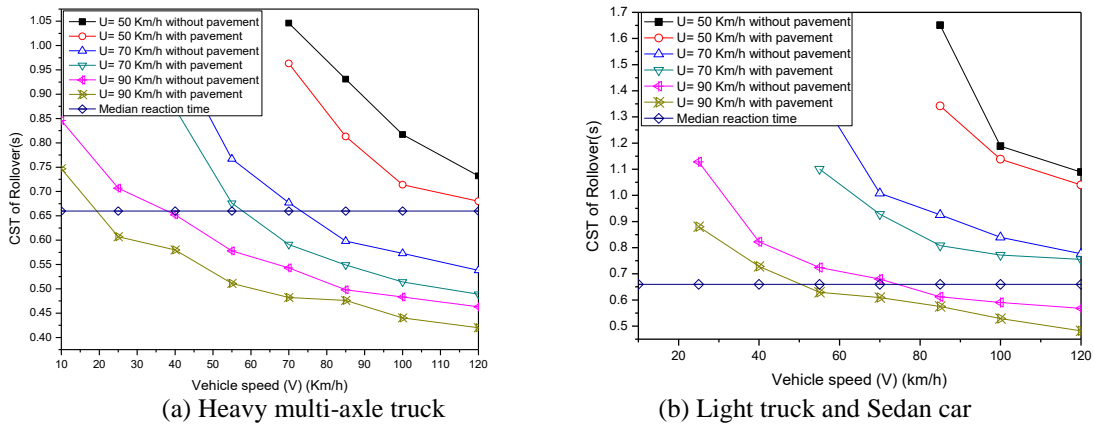
Fig. 10 Effect of pavement on the CST of rollover accident on the dry surface of bridge

(a) Heavy multi-axle truck   (b) Light truck and Sedan car
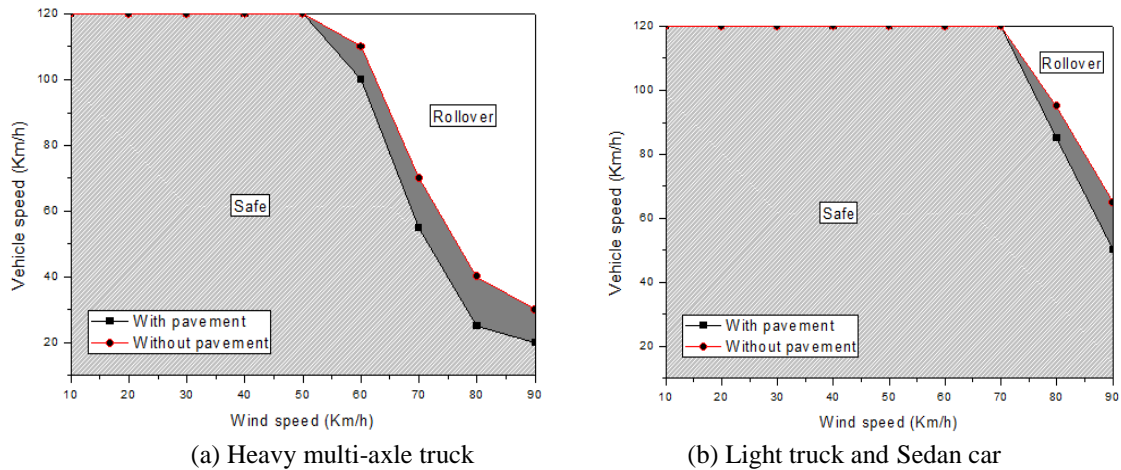
Fig. 11 Effect of pavement on the CDS of rollover accident on the dry surface of bridge

It can be found from Fig. 9 that when the vehicle moves on the snow-covered surface, the sideslip accident may happen very easily, and it is easy to find that the sideslip accidents will happen when U and V are not high. When the wind speed is more than 50 km/h, sideslip accidents will happen when the truck moves with 42 km/h. When the wind speed is more than 80 km/h, even the truck in still V=10 km/h will have the risk of being sideslip. By comparing Figs. 8 and 9, it is obvious that sideslip accidents will be more prone to occur first than rollover accidents when the road kinetic friction coefficient decreases.

7.4 Effect of pavement on the CST and CDS of accidents

As discussed earlier, the effect of pavement on the ride safety is significant. Using the present model of wind-traffic-pavement-bridge coupled vibration system, the effect of pavement and traffic flow on the CST and CDS of accidents were studied and plotted in Figs. 10 and 11.

Figs. 10 and 11 show that the effects of pavement on the CST and CDS of accidents. It can be found from Fig. 10 that the pavement can decrease the CST of accidents, for instance, when the pavement is considered for the truck, the CST of accidents diseases from 0.82s to 0.71 s for the wind speed is 50 km/h and vehicle speed is 100km/h. It can be found from Fig. 11 that the pavement can increase the CDS of accidents, for instance, when the pavement is considered for the truck, the CST of accidents increases from 55 km/h to70 km/h. Therefore, the effects of pavement on the CST and CDS of accidents should be considered for giving the more precisely simulating results.

7.5 Effect of traffic flow occupancies on the CST and CDS of accidents

The Transportation Research Board classifies the "level of service" from a driving operation under a desirable condition to an operation under forced or breakdown conditions (Chen and Wu 2010). In following sections, two traffic flow occupancies, including the median traffic ρ =0.15 and busy traffic flow ρ =0.3 (Chen and Wu 2010), are used to study the CST and CDS of

(a) Heavy multi-axle truck　　　　(b) Light truck and Sedan car
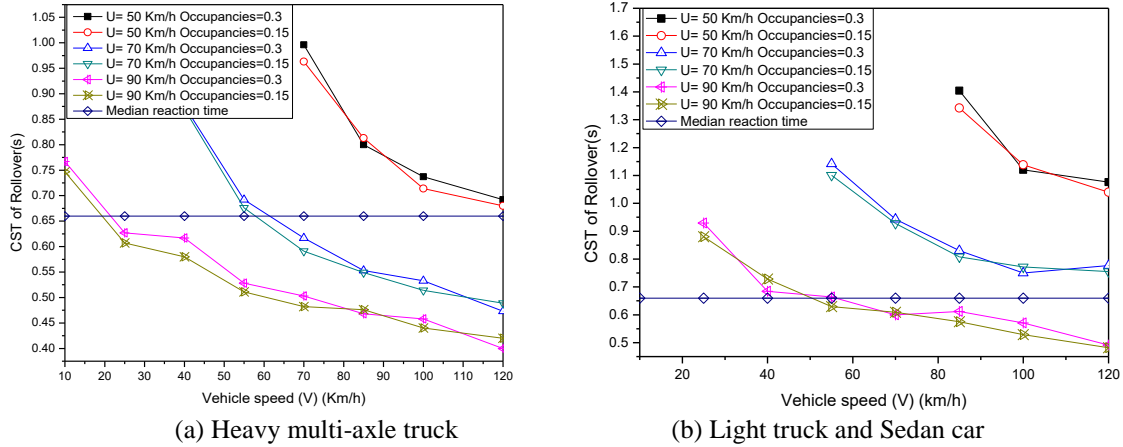
Fig. 12 Effect of flow occupancy on the CST of rollover accident on the dry surface of bridge

(a) Heavy multi-axle truck　　　　(b) Light truck and Sedan car
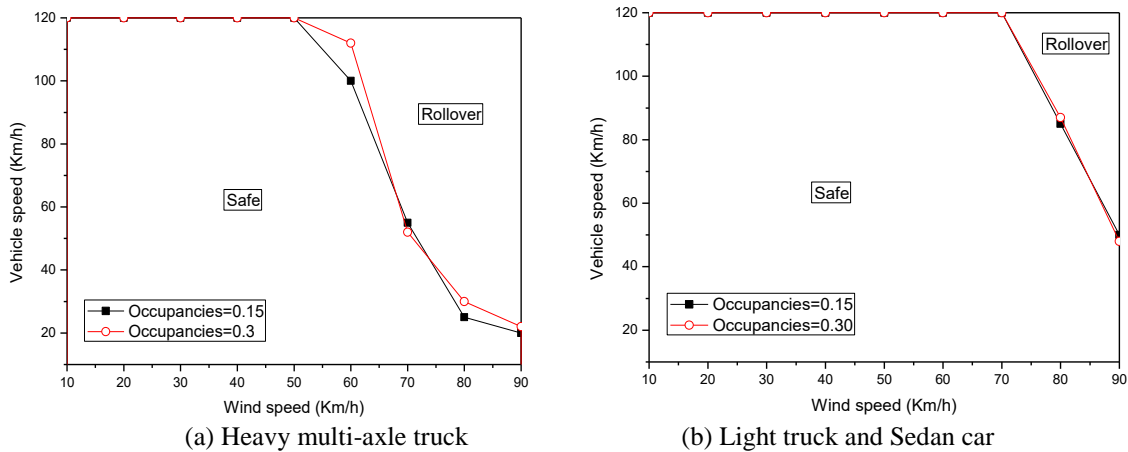
Fig. 13 Effect of flow occupancy on the CDS of rollover accident on the dry surface of bridge

accidents of the bridge under the dry surface roughness. The CST and CDS of accidents are shown in Figs. 12 and 13.

It is found from Figs. 12 and 13 that traffic flow occupancies play a not more significant role on the CST and CDS of accidents. For example, when the wind speed is 70 km/h, and two traffic flow occupancies, including the median traffic and busy traffic flow, are considered respectively, the CST of accidents are 0.62s and 0.59s cm, respectively, and the CDS of accidents are 55 km/h and 52 km/h, , respectively. Therefore, from this numerical example, the changing degree of CST and CDS of accidents by considering the traffic flow occupancies is not more significant.

8. Conclusions

This paper presents a new assessment simulation of ride safety based on a new

wind-traffic-pavement-bridge coupled vibration system. Compared to existing simulation models, the new coupled system focuses on introducing the more realistic three-dimensional vehicle model, pavement simulation, stochastic characteristics of traffic, vehicle accident criteria, and bridge surface roughness. The numerical simulations show that the proposed method can rationally provide useful assessment information for traffic, and define appropriate safe driving speed limits for vulnerable vehicles under normal and busy traffic conditions. The following conclusions can be drawn:

(1) The CST of accidents is an important assessment criterion for the ride safety, considering the CST of accident and median reaction time of drivers, some accident may not actually happen;

(2) The effect of wind speed on the CST and CDS of accidents is very significant, the CST and CDS of accidents decreases with the wind speed increasing;

(3) The pavement can decrease the CST of accidents, and the pavement can increase the CDS of accidents, therefore, the effects of pavement on the CST and CDS of accidents should be considered for giving the more precisely simulating results;

(4) From this numerical example, the changing degree of CST and CDS of accidents by considering the traffic flow occupancies is not more significant.

Acknowledgments

References

AASHTO. (2004), A policy on geometric design of highways and streets, AASHTO, Washington, D.C.

Andersen, L., Nielsen, S.R.K. and Kirkegaard, P.H. (2001), "Finite element modeling of infinite Euler beams on Kelvin foundations exposed to moving loads in converted coordinates", *J. Sound Vib.*, **241**(4), 587-604.

Baker, C.J. (1991), "Ground vehicles in high cross winds. Part I: Unsteady aerodynamic forces", *J. Fluids Struct.*, **5**, 91-111.

Cai, C.S., Hu, J., Chen, S., Han, Y., Zhang, W. and Kong, X. (2015), "A coupled wind-vehicle-bridge system and its applications: a review", *Wind Struct.*, **20**(2), 117-142.

Cao, Z., Cai, Y., Sun, H. and Xu, C. (2011), "Dynamic responses of a poroelastic half-space from moving trains caused by vertical track irregularities", *Int. J. Numer. Anal. Methods Geomech.*, **35**(7), 761-786.

Chen, S.R. and Cai, C.S. (2004), "Accident assessment of vehicles on long-span bridges in windy environments", *J. Wind Eng. Ind. Aerod.*, **92**(12), 991-1024.

Chen, S.R. and Cai, C.S. (2007), "Equivalent wheel load approach for slender cable-stayed bridge fatigue assessment under traffic and wind: feasibility study", *J. Bridge Eng.*, **12**(6), 755-764.

Chen, S.R. and Chen, F. (2010), "Simulation-based assessment of vehicle safety behavior under hazardous driving conditions", *J. Bridge Eng.*, **136**(4), 304-315.

Chen, S.R. and Wu, J. (2010), "Dynamic performance simulation of long-span bridge under combined loads of stochastic traffic and wind", *J. Bridge Eng.*, **15**(3), 219-230.

Chen, S.R. and Wu, J. 2011), "Modeling stochastic live load for long-span bridge based on microscopic traffic flow simulation", *Comput. Struct.*, **89**, 813-824.

Chen, Y.B. and Feng, M.Q. (2006), "Modeling of traffic excitation for system identification of bridge structures", *Comput. - Aided Civil. Infrastruct. Eng.*, **21**, 57-66.

Clough, R.W. and Penzien, J. (1993), "Dynamics of structures", New York, McGraw-Hill Inc.

Deng, L. and Wang, F. (2014), "Impact factors of simply-supported prestressed concrete girder bridges due to vehicle braking", *J. Bridge Eng. - ASCE*, 10.1061/(ASCE) BE.1943-5592. 0000764 , 06015002.

Deng, L., Yu, Y., Zou, Q.L. and Cai, C.S. (2014), "State-of-the-art review on dynamic impact factors of highway bridges", *J. Bridge Eng. - ASCE*, 10.1061/(ASCE)BE.1943-5592.0000672 , 04014080. (SCI)

Fujii, S. and Yoshimoto, K. (1975), "An analysis of the lateral hunting motion of a two-axle railway wagon by digital simulation (1st report, the outline of the mathematical model)", *Bull. JSME*, **18**(122), 813-818.

Fujii, S., Yoshimoto, K. and Kobayashi, F. (1975), "An analysis of the lateral hunting motion of a two-axle railway wagon by digital simulation (2nd report, the outline of the mathematical model)", *Bull. JSME*, **18**(125), 1246-1251.

Gim, G. and Nikravesh, P.E. (1990), "Analytical model of pneumatic types for vehicle dynamic simulations Part 1. Pure slips", *Int. J. Vehicle Des.*, **11**(5), 589-618.

Han, W., Ma, L., Cai, C.S., Chen, S. and Wu, J. (2015) "Nonlinear dynamic performance of long-span cable-stayed bridge under traffic and wind", *Wind Struct.*, **20**(2), 249-274.

Han, Y., Hao Chen, C.S. Cai and Guoji Xu, Lian Shen, Peng Hu (2016), "Numerical analysis on the difference of drag force coefficients of bridge decksections between the global force and pressure distribution methods", *J. Wind Eng. Ind. Aerod.*, **159**, 65-79.

ISO. (1995), "Mechanical vibration-road surface profiles-reporting of measured data", ISO 8068: (E), Geneva.

Liu, Y.,Yin, X., Deng, L. and Cai, C.S. (2016), "Ride comfort of the bridge-traffic-wind coupled system considering bridge surface progressive deterioration", *Wind Struct.*, **23**(1), 19-43.

Mamlouk, M.S. (1997), "General outlook of pavement and vehicle dynamics", *J. Transport. Eng.*, **123**(6), 515-517.

Nagel, K. and Schreckenberg, M. (1992), "A cellular automaton model for freeway traffic", *J. Phys.* (France), **2**(12), 2221–2229.

Park, J.H., Huynh, T.C., Lee, K.S. and Kim, J.T. (2016), "Wind and traffic-induced variation of dynamic characteristics of a cable-stayed bridge–benchmark study", *Smart Struct. Syst.*, **17**(3), 491-522.

Xianjuan, K., Ziyou, G. and Keping, L. (2006), "A two lane celluar automata model with influence of next nearest neighbor vehicle", *Commun. Theoretical Phys.*, **45**(4), 657-662.

Xu, Y.L. and Guo, W.H. (2004), "Effects of bridge motion and crosswind on ride comfort of road vehicles", *J. Wind Eng. Ind. Aerod.*, **92**, 641-662.

Yin, X.F., Fang, Z. and Cai, C.S. (2011), "Lateral vibration of high-pier bridges under moving vehicular loads", *J. Bridge Eng.*, **16**(3), 400-412.

Yin, X.F., Liu, Y., Guo, S. and Cai C.S.(2016), "Three-dimensional vibrations of a suspension bridge under stochastic traffic flows and road roughness", *Int. J. Struct. Stab. Dynam.*, 16:1550038. DOI: 10.1142/S0219455415500388.

CC